JUSAN SCIENCE

Journal of Engineering and Environmental Systems

ISSN (Print): 3135-2510; ISSN (Online): 3135-2529

journal homepage: https://jusanscience.com/journals/jees

Research Article

Selective Benzene Hydrogenation over Ru Catalysts in Multi-Aromatic Mixtures

Aiken Manassova[1], Rachid Amrousse[2], Kainaubek Toshtay[1*]

[1]Al-Farabi Kazakh National University, Al-Farabi 71, Almaty, 050040, Kazakhstan
[2]Chouaïb Doukkali University, Faculty of Sciences, 24000 El Jadida, Morocco

Corresponding author: Kainaubek Toshtay kainaubek.toshtay@kaznu.kz

https://doi.org/10.66973/jees.26.003

Article info:

Received: 10 March 2026 / Revised: 20 March 2026 / Accepted: 22 March 2026 / Published: 30 March 2026

Manassova, A., Amrousse, R., Toshtay, K. (2026). Selective Benzene Hydrogenation over Ru Catalysts in Multi-Aromatic Mixtures. *Journal of Engineering and Environmental Systems*, 1, 27-41. https://doi.org/10.66973/jees.26.003

Abstract: Ruthenium catalysts supported on diatomite (Ru/D) with varying loadings (0.5–1.5 wt.%) were synthesized and evaluated for the selective hydrogenation of aromatic compounds. Characterization by SEM, TEM, EDX, XRD, and BET revealed that the diatomite support retains its highly porous structure after Ru deposition, enabling uniform dispersion of Ru nanoparticles. EDX confirmed Ru incorporation, while XRD indicated the presence of highly dispersed Ru nanoclusters below the detection limit. Textural analysis showed a gradual decrease in surface area (60–45 $m^2\ g^{-1}$) and pore volume (0.08–0.07 $cm^3\ g^{-1}$) with increasing Ru content, consistent with partial pore filling. Hydrogenation studies demonstrated that catalytic activity increased with Ru loading, with 1.5% Ru/D exhibiting the highest benzene hydrogenation rate (≈20×10^{-6} $mol.s^{-1}$). Benzene hydrogenation followed Arrhenius behavior, yielding an apparent activation energy of ~60 $kJ\ mol^{-1}$. Toluene and o-xylene hydrogenation showed slower kinetics due to steric and electronic effects of methyl substituents, while selectivity studies on a mixture of aromatics indicated nearly complete benzene conversion (94%) with minimal hydrogenation of substituted aromatics (toluene 14%, o-xylene 2%).

Keywords: hydrogenation; ruthenium catalyst; diatomite; benzene; toluene; o-xylene.

1 Introduction

Catalytic hydrogenation of benzene is one of the key processes in modern petroleum refining and environmental protection technologies. The principal source of benzene in motor fuels is the catalytic reforming process, in which the benzene concentration in the reformate stream can sometimes reach 10–14 % [1]. Additional sources of benzene include pyrolysis gasoline and cracking products, which can further increase its concentration in fuel streams. Without additional purification, the benzene content in gasoline may significantly exceed the current environmental limits, which are restricted to ≤1 % in Europe and the United States [2], [3].

Benzene is a highly toxic aromatic hydrocarbon with pronounced carcinogenic properties. According to the classification of the International Agency for

https://doi.org/10.66973/jees.26.003

Research on Cancer, benzene belongs to Group 1 carcinogens, meaning that it is carcinogenic to humans. Incomplete combustion of benzene-containing fuels can lead to the formation of polycyclic aromatic hydrocarbons, including highly hazardous compounds such as benzo[a]pyrene (Figure 1). These compounds can accumulate in soil and vegetation and exert mutagenic and carcinogenic effects even at very low concentrations [4], [5]. For this reason, modern fuel quality standards, including those defined by the Euro 5 and Euro 6 emission standards, strictly limit the benzene content in gasoline to no more than 1% [6], [7]. Among the available technologies, catalytic hydrogenation is considered one of the most effective methods for reducing benzene content in motor fuels.

Beyond environmental considerations, benzene hydrogenation is also important for the production of valuable industrial chemicals. The main hydrogenation products-cyclohexane and cyclohexene-serve as key intermediates in the manufacture of nylon-6 and nylon-6,6, as well as in the production of solvents and plasticizers [8], [9]. In addition, the benzene-cyclohexane pair has recently attracted considerable attention as a promising liquid organic hydrogen carrier system. In this concept, hydrogen can be stored via benzene hydrogenation to cyclohexane and subsequently released through catalytic dehydrogenation. Cyclohexane contains approximately 7.2 wt.% hydrogen, enabling efficient hydrogen storage and reversible cycling between the two compounds [10], [11].

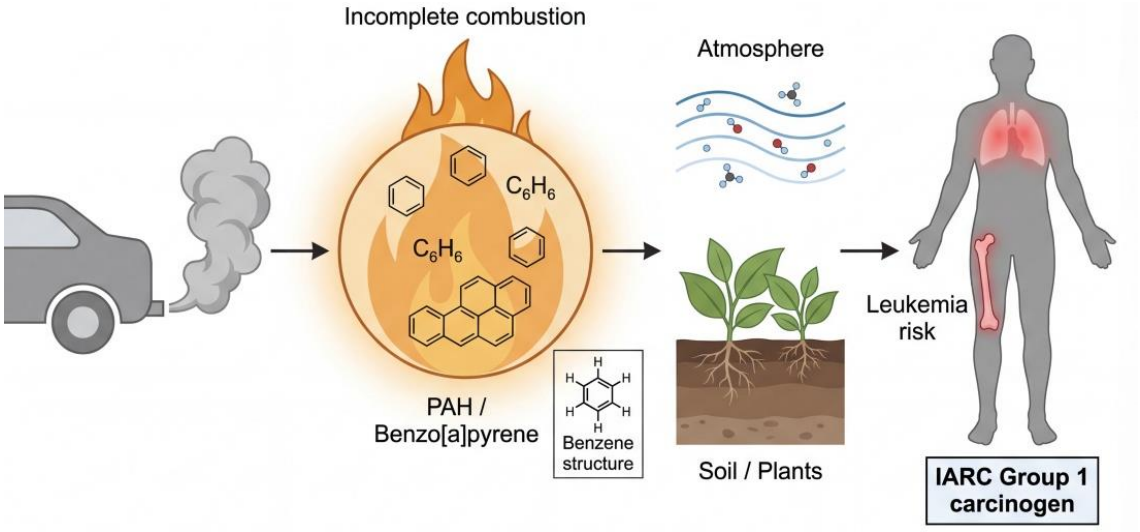

Figure 1. Pathway of polycyclic aromatic hydrocarbons from incomplete combustion to human health risks.

Despite its importance, selective hydrogenation of benzene in the presence of other aromatic compounds remains a significant scientific and technological challenge. The strong π-conjugation of the benzene ring results in a relatively high activation energy for hydrogenation. At the same time, alkyl-substituted aromatics such as toluene and xylenes often exhibit stronger adsorption on catalyst surfaces than benzene, thereby blocking active sites and suppressing benzene conversion [12], [13]. Furthermore, gasoline fractions typically contain olefins, which are hydrogenated much more readily than benzene. As a result, many catalysts preferentially hydrogenate C=C bonds, leading to undesirable reduction of the fuel octane number [14], [15]. Achieving high selectivity under such competitive conditions therefore requires careful optimization of catalyst composition, support structure, and reaction parameters.

A variety of catalysts based on Ni, Pd, Pt, Ru, and Rh have been extensively investigated for benzene hydrogenation [16]. Nickel-based catalysts, particularly Ni/Al_2O_3 systems, are widely used in industry due to their relatively low cost and high activity; however, their selectivity toward benzene in the presence of other aromatic compounds is often limited [17], [18]. Palladium catalysts can demonstrate relatively high benzene selectivity (up to ~76%) under elevated hydrogen pressures [19]. Ruthenium-based catalysts are particularly attractive due to their excellent ability to dissociatively adsorb

hydrogen and achieve high conversion under relatively mild conditions (60–120 °C and 2–5 MPa) [20], [21].

In this context, the present study focuses on the preparation of ruthenium-based catalysts supported on natural diatomite and the evaluation of their catalytic performance in the hydrogenation of aromatic hydrocarbons, including benzene, toluene, o-xylene, and their mixtures. Special attention is given to the influence of ruthenium loading on the structural properties and catalytic activity of the prepared catalysts. The effect of reaction temperature on the hydrogenation rate and product selectivity is also investigated.

2 Experimental part

2.1 Materials

Ruthenium(III) chloride trihydrate ($RuCl_3 \cdot 3H_2O$) was used as the metal precursor for catalyst preparation. Diatomite served as the catalyst support. The natural diatomite was obtained from the Mughalzhar deposit (Kazakhstan). Prior to use, the raw material was dried, sieved, and the fraction with a particle size below 100 μm was collected for further processing. Benzene, toluene and o-xylene was selected as the model hydrogenation substrate, while ethanol was employed as the reaction solvent.

2.2 Catalyst Preparation

Natural diatomite contains surface impurities that hinder the deposition of active metal species and consequently decrease the catalytic performance of the material. Therefore, prior to catalyst synthesis, the diatomite was subjected to acid activation followed by thermal treatment [22], [23]. A 10 wt.% hydrochloric acid solution was first prepared by diluting concentrated HCl with deionized water under continuous stirring. The appropriate amount of natural diatomite was then added to the acid solution, maintaining a diatomite-to-solution mass ratio of 1:3. The suspension was stirred at 80 °C for 2 h to ensure effective removal of surface impurities and partial dealumination. After acid treatment, the solid was separated by filtration, thoroughly washed if necessary, and calcined in air at 500 °C for 3 h. The calcined material was subsequently ground in a ball mill to obtain a homogeneous fine powder. X-ray fluorescence (XRF) analysis revealed that the activated diatomite (hereafter denoted as D) consisted predominantly of SiO_2 (87.9 wt.%) and Al_2O_3 (9.8 wt.%). Ruthenium-supported catalysts were prepared using an impregnation-assisted hydrothermal method and are denoted as Ru/D. In a typical procedure, the required amount of activated diatomite (D) was dispersed in an aqueous solution of $RuCl_3 \cdot 3H_2O$ and stirred for 30 min to promote uniform distribution of the precursor. The resulting suspension was transferred into a stainless-steel autoclave, sealed tightly, and subjected to hydrothermal treatment at 120 °C for 10 h. After cooling to room temperature, the solid product was recovered by filtration using a ceramic filter and thoroughly washed with distilled water to remove residual chloride ions. The obtained material was dried under vacuum at 60 °C overnight. Prior to catalytic evaluation, the Ru/D samples were reduced in a hydrogen atmosphere at 400 °C for 1 h to generate the metallic active phase.The nominal ruthenium loadings in the catalysts were 0.5, 1.0, and 1.5 wt.%.

2.3 Catalyst Characterization

The microstructural features of the samples were investigated using field-emission scanning electron microscopy (FE-SEM, Hitachi SU8010) operated at an accelerating voltage of 15 kV. Both secondary electron and backscattered electron imaging modes were employed to evaluate the surface morphology and compositional contrast.

The crystalline structure and phase composition were analyzed by powder X-ray diffraction (XRD) using a D8 Advance A25 diffractometer (Bruker) equipped with Cu Kα radiation (λ = 0.1540 nm) and a Ni filter. Diffraction patterns were recorded over a 2θ range of 4–80° with a step size of 0.02°. Phase identification was performed by comparison with reference patterns from the JCPDS database.

The textural properties were determined from nitrogen adsorption–desorption measurements carried out at 77 K using an ASAP 2020 surface area and porosity analyzer (Micromeritics). Prior to analysis, the samples were degassed under vacuum at 300 K to remove physically adsorbed species. The

https://doi.org/10.66973/jees.26.003

specific surface area was calculated according to the Brunauer–Emmett–Teller (BET) method, while the pore size distribution was derived from the desorption branch of the isotherm using the Barrett–Joyner–Halenda (BJH) model [24].

The bulk ruthenium content was quantified by inductively coupled plasma optical emission spectroscopy (ICP–OES, Optima 3300DV, PerkinElmer).

The morphology, dispersion, and particle size distribution of the supported Ru species were further examined by transmission electron microscopy (TEM, JEM-2010, JEOL, Japan) operated at 200 kV with a point resolution of 0.14 nm. For TEM analysis, the samples were ultrasonically dispersed in ethanol and deposited onto carbon-coated copper grids.

2.4 Hydrogenation methods

The pre-crushed catalyst (0.6 g) was loaded into the reactor, followed by the addition of 1.0 mL of benzene, toluene, or xylene, and 60 mL of ethanol. The reactor was sealed and purged with nitrogen to remove air. The temperature was then set within the range of 90-130 °C. After reaching the desired temperature, the reactor was purged with hydrogen, the pressure was adjusted to 2.0 MPa, and mechanical stirring was initiated at 800 rpm. During the catalytic experiment, samples of the reaction mixture were withdrawn at predetermined time intervals. The reaction rate was determined using the volumetric method [25]. The hydrogenation rate (W) was calculated using the following formula (1):

$$W = \frac{(V_f\text{-}V_i).a}{(t_f\text{-}t_i)} \qquad W = \frac{\Delta V_o.a}{\Delta t} \tag{1}$$

where V_i and V_f are the initial and final amounts of absorbed hydrogen (mol), Δt is the time interval over which the rate is determined (s), and a is a coefficient accounting for the system pressure. The reaction products were analyzed using a Chromos gas chromatograph equipped with a flame ionization detector (FID) and a PEG-20M capillary column (0.25 mm diameter, 30 m length).

3 Results and discussion

3.1 catalyst characterization

Figure 2 shows the SEM images and corresponding EDX spectra of Ru catalysts supported on diatomite with different Ru loadings: (a) 0.5%Ru/D, (b) 1.0%Ru/D, and (c) 1.5%Ru/D.

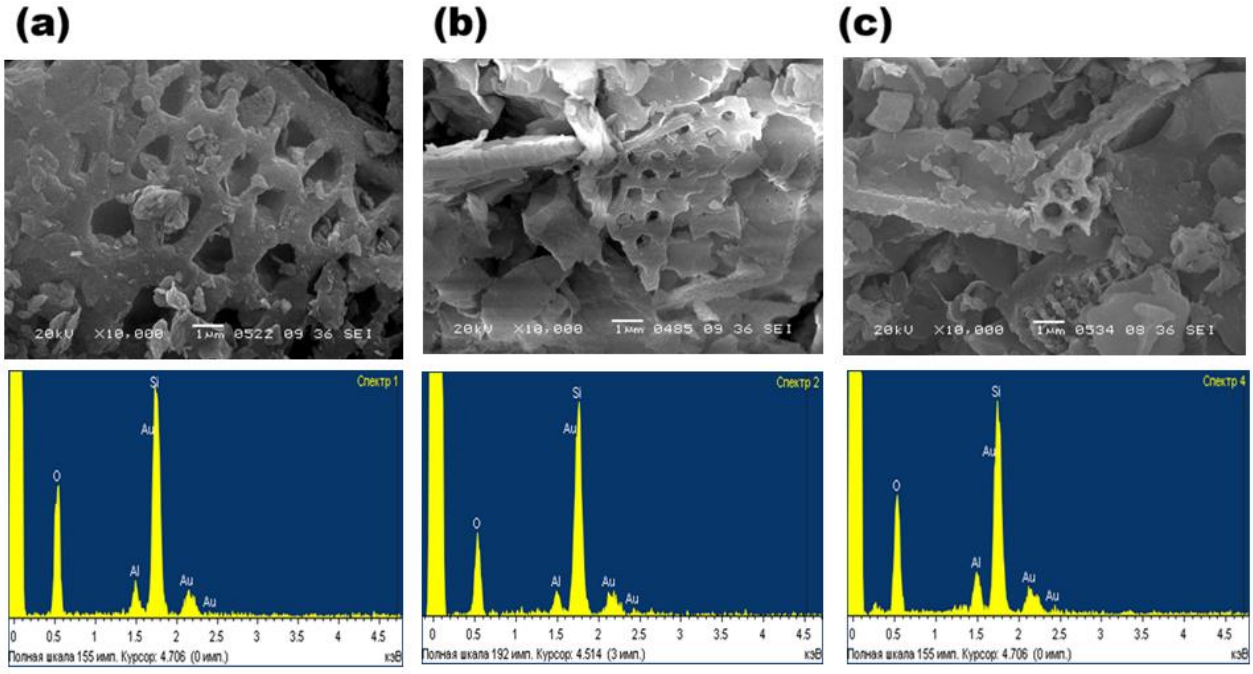

Figure 2. SEM images and EDX spectra of the catalysts: (a) 0.5%Ru/D, (b) 1.0%Ru/D, (c) 1.5%Ru/D.

https://doi.org/10.66973/jees.26.003

The SEM images reveal that the diatomite support possesses a highly porous and irregular structure, typical of silica-based diatomaceous materials. Such morphology provides a large surface area and numerous pores, which are beneficial for the dispersion of active metal particles and for mass transfer during catalytic reactions. For all catalysts, the characteristic porous framework of diatomite is preserved after Ru deposition, indicating that the impregnation process does not significantly alter the support structure. At higher Ru loading (1.5% Ru/D), the surface appears slightly denser, which may suggest partial aggregation of metal species.

The EDX spectra confirm the presence of the main elements in the catalysts. Strong peaks of Si and O originate from the silica-rich diatomite support, while minor Al signals correspond to natural impurities in the material. The detection of Ru peaks indicates the successful deposition of ruthenium on the support. A small Au signal is also observed, which is attributed to the gold coating applied during SEM sample preparation. Overall, the results confirm that Ru was successfully supported on the porous diatomite structure without significant structural changes.

Figure 3 shows TEM images of Ru catalysts supported on diatomite with different Ru loadings: (a) 0.5% Ru/D, (b) 1.0% Ru/D, and (c) 1.5% Ru/D. The TEM micrographs reveal that Ru nanoparticles are distributed on the surface of the diatomite support. In the 0.5% Ru/D catalyst (Figure 3a), very small and well-dispersed Ru particles can be observed, indicating a high dispersion of the active metal at low loading. The particles appear as fine dark spots uniformly distributed across the support surface. For the 1.0% Ru/D catalyst (Figure 3b), the number of visible Ru nanoparticles increases, while the particles remain relatively well dispersed. This suggests that the diatomite support provides sufficient anchoring sites for the metal particles, preventing significant agglomeration. In the 1.5% Ru/D catalyst (Figure 3c), the density of Ru nanoparticles on the support surface becomes noticeably higher, and several larger particles can be observed. This indicates that partial aggregation of Ru nanoparticles occurs at higher metal loading, which is a common phenomenon in supported metal catalysts.

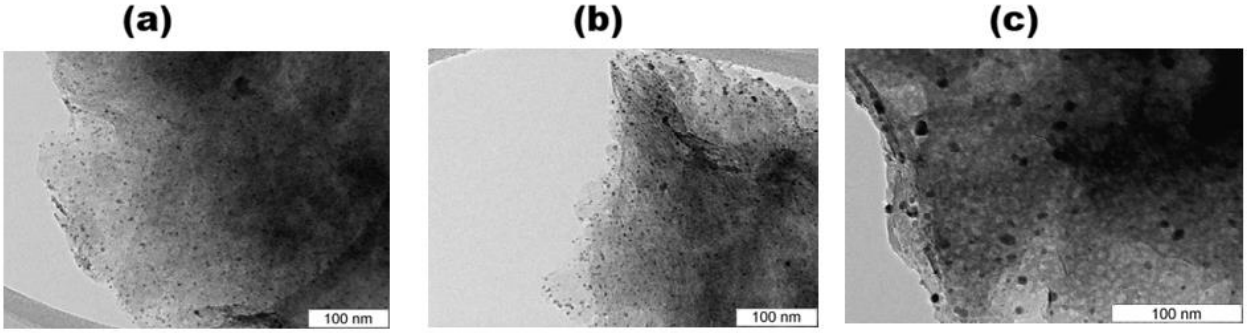

Figure 3. TEM images of the catalysts: (a) 0.5%Ru/D, (b) 1.0%Ru/D, and (c) 1.5%Ru/D.

The deposition of Ru onto the D support is accompanied by a gradual decrease in the specific surface area (from 60 to 45 $m^2\ g^{-1}$) and the total pore volume (from 0.08 to 0.07 $cm^3\ g^{-1}$), as well as a slight reduction in the average pore diameter (from 19 to 18 nm, Table 1). This behavior indicates partial filling of the pores by ruthenium species, confirming the successful incorporation of the active phase onto the support. Furthermore, the actual Ru content closely matches the nominal loading values. Figure 4 presents the XRD patterns of the D support and Ru/D catalysts with different ruthenium loadings (0.5, 1.0, and 1.5 wt.%). The XRD analysis of the diatomite sample (D) revealed the presence of crystalline peaks corresponding to phases containing silicon dioxide (quartz and opal), as well as clay minerals (illite and kaolinite). The diffractogram of the original support shows well-defined reflections of these minerals, while the amorphous silica phase typical for diatomites appears as a broad, non-structured background. The obtained results confirm that the structure of diatomite retains the crystallinity of individual components while simultaneously containing a significant fraction of amorphous SiO_2,

https://doi.org/10.66973/jees.26.003

which is characteristic of natural diatomaceous rocks [26], [27], [28].

Table 1. Textural properties of the prepared catalysts.

Sample	S_{BET} (m^2 g^{-1})	Average pore diameter (nm)	Pore volume (cm^3 g^{-1})	Actual Ru content (%)
D	60.0	19.0	0.08	—
0.5%Ru/D	57.0	19.0	0.08	0.48
1.0%Ru/D	50.0	19.0	0.07	0.96
1.5%Ru/D	45.0	18.0	0.07	1.47

For the catalysts modified with different ruthenium contents (0.5–1.5 wt.% Ru/D), the XRD patterns practically coincide with that of the original diatomite. The positions and intensities of the main peaks correspond to the phases of quartz and clay minerals, indicating that the crystalline structure of the support is preserved after the deposition of the active component. Characteristic diffraction reflections of ruthenium are not observed in the presented patterns. This can be attributed to the extremely low Ru concentration and its high degree of dispersion, as a result of which the metal is present in the form of nanoclusters or sub-nanometer particles whose sizes are below the detection limit of conventional powder XRD.

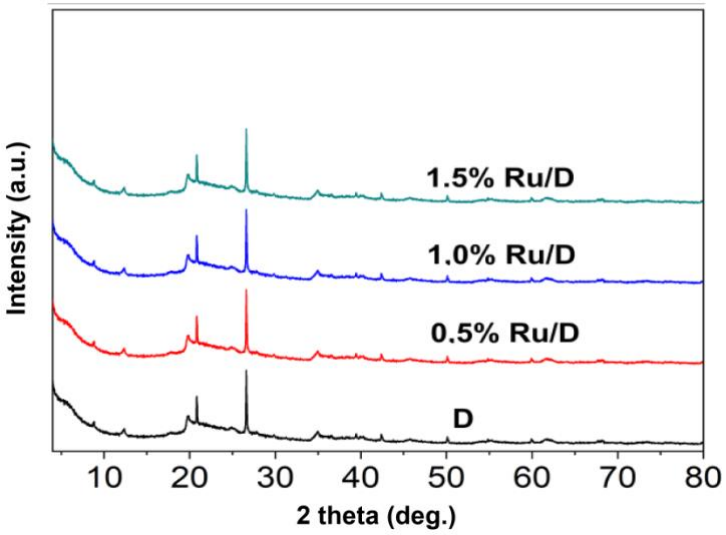

Figure 4. XRD patterns of diatomite (D) and Ru/D catalysts with different Ru loadings.

3.2 Hydrogenation of benzene.

Figure 5 shows the dependence of the benzene hydrogenation reaction rate over the 1.0 wt.% Ru/D catalyst on the volume of absorbed hydrogen at different temperatures (90, 110, and 130 °C). For all investigated temperatures, typical curves are observed: the reaction rate initially increases with increasing hydrogen uptake, reaching a certain plateau, after which it gradually decreases.

At 90 °C, the maximum reaction rate is achieved at a relatively low hydrogen uptake (~300–350 mL), which reflects the limited catalytic activity at lower temperature and the relatively slow saturation dynamics of the active sites. Increasing the temperature to 110 °C leads to an increase in both the reaction rate and the hydrogen volume corresponding to maximum activity. This indicates more efficient participation of the Ru active sites in the hydrogenation process. The highest reaction rate values are observed at 130 °C. The maximum of the

https://doi.org/10.66973/jees.26.003

curve shifts toward higher degrees of hydrogenation, indicating an increase in the number of active sites involved in the reaction, as well as an intensification of mass-transfer processes. However, a further increase in hydrogen uptake leads to a decrease in the reaction rate, which may be due to partial blockage of active sites by excessively adsorbed hydrogen or to limitations in substrate diffusion.

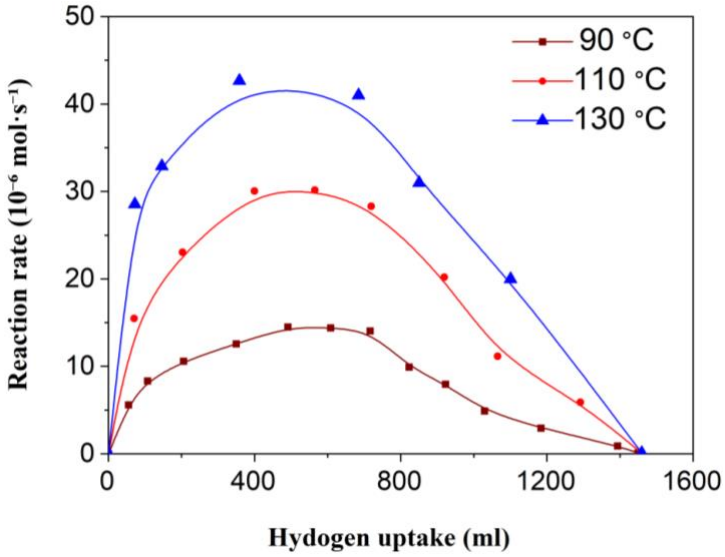

Figure 5. Dependence of the reaction rate on hydrogen uptake during benzene hydrogenation over the 1.0 % Ru/D catalyst.

Figure 6 presents the Arrhenius plot showing the logarithmic dependence of the reaction rate constant (lg k) on the reciprocal temperature (1000/T) for benzene hydrogenation over the studied catalyst. A linear relationship between lg k and 1000/T is observed within the investigated temperature range, indicating that the reaction follows the Arrhenius law. The decrease in lg k with increasing 1000/T corresponds to an increase in the reaction rate constant with increasing temperature, which is typical of thermally activated catalytic processes.

The slope of the straight line was used to estimate the apparent activation energy of the reaction, which was calculated to be approximately 50 kJ mol^{-1}. The good linear correlation of the experimental data suggests that the hydrogenation process proceeds through a consistent kinetic mechanism under the studied conditions. These determined activation energy values are consistent with those reported by the authors in [29], [30].

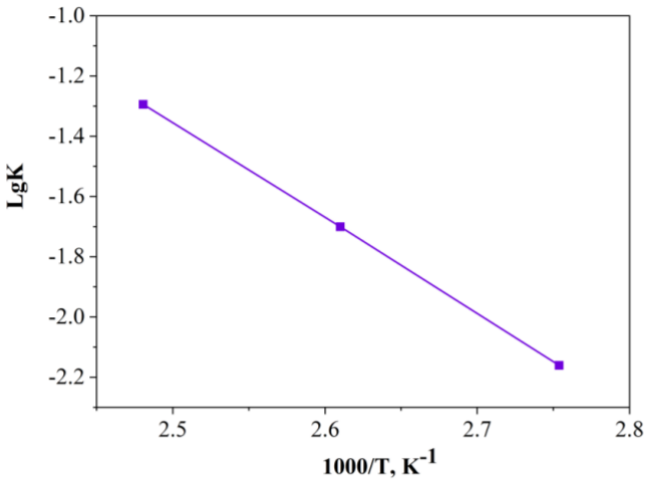

Figure 6. Logarithmic dependence of the rate constant on the reciprocal temperature.

Figure 7 presents the kinetic curves of benzene hydrogenation over catalysts with different ruthenium (Ru) loadings, expressed as percentages (0.5%, 1.0%, and 1.5% Ru/D). The experiment was carried out at a temperature of 90 °C.

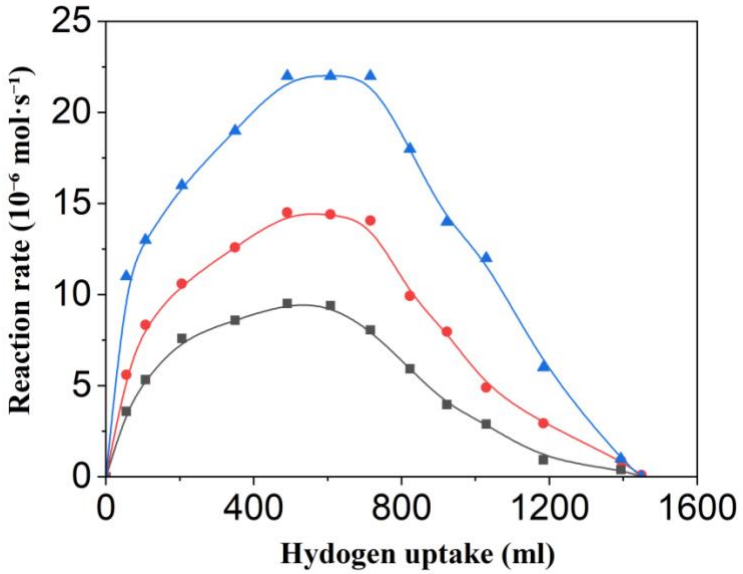

Figure 7. Kinetic curves of benzene hydrogenation over Ru/D catalysts with Ru loadings of 0.5%, 1.0%, and 1.5% at 90 °C.

It can be seen that in all cases a sharp initial increase in the reaction rate is observed as hydrogen is absorbed, after which the rate reaches a plateau. At the same time, the catalytic activity significantly increases with increasing ruthenium content. In particular, the catalyst containing 1.5% Ru/D exhibits the highest reaction rate (above 20×10^{-6} mol.s^{-1}), which is almost twice as high as that observed for the sample containing 0.5% Ru/D. The catalyst with 1.0% Ru/D shows intermediate activity. The obtained results indicate that an increase in Ru concentration promotes the formation of a larger number of active sites, which leads to an enhancement of the benzene hydrogenation rate.

3.3 Hydrogenation of Toluene.

The catalytic hydrogenation of toluene involves the saturation of the aromatic ring, resulting in the formation of methylcyclohexane. Typically, this process is carried out over noble metal catalysts (Ru, Pt, Pd) or Ni-based catalysts under elevated hydrogen pressures (2–10 MPa) and at temperatures ranging from 80 to 200 °C.

The reaction mechanism is similar to that of benzene: initially, the toluene molecule adsorbs onto the metal surface, weakening its π-system, after which hydrogen atoms gradually add to the ring. The methyl group is generally preserved, making methylcyclohexane the main product. Depending on the nature of the catalyst, temperature, and pressure, side products such as cracking products, isomers, or dimethylcyclopentanes may also form [31], [32].

Hydrogenation experiments of toluene were conducted at 90 °C under 1 MPa hydrogen pressure (800 rpm) in an ethanol solvent. The results of the hydrogenation are shown in Figure 8.

As seen in Figure 8, the reaction rate during toluene hydrogenation initially increases sharply during the early stages of hydrogen uptake, reaching a maximum at approximately 200–300 mL of hydrogen absorbed, and then gradually decreases. This behavior is observed at all temperatures tested (90, 110, and 130 °C), indicating that at the beginning of the process, the active sites on the catalyst surface are fully accessible and adsorption of both hydrogen

https://doi.org/10.66973/jees.26.003

and toluene is optimal. As the reaction proceeds, the accumulation of products and surface saturation lead to a decline in the reaction rate.

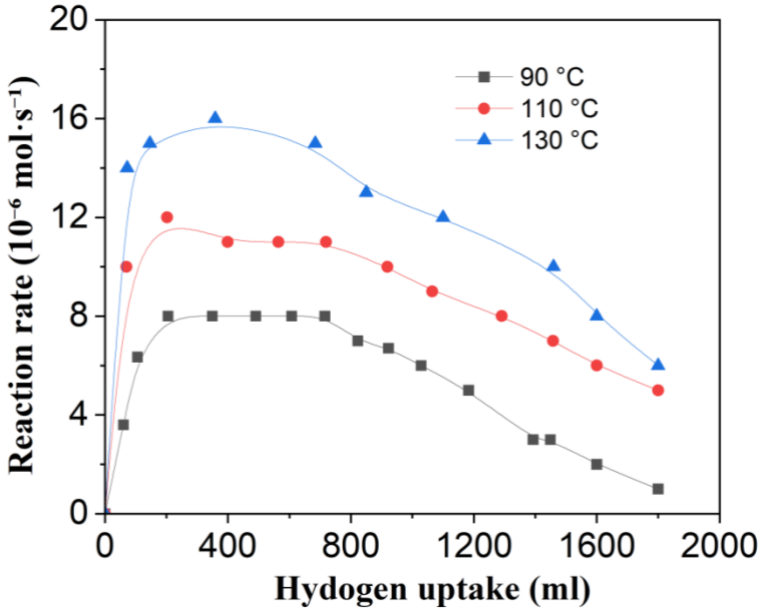

Figure 8. Dependence of the reaction rate on hydrogen uptake during toluene hydrogenation over 1.0% Ru/D catalyst at different temperatures.

The reaction rate increases significantly with temperature: at 130 °C, the maximum rate (~16 × 10^{-6} mol s^{-1}) is almost twice as high as at 90 °C and higher than at 110 °C. Throughout the entire range of hydrogen uptake, the rate follows the order 130 °C > 110 °C > 90 °C. This indicates that raising the temperature to 110–130 °C markedly accelerates toluene hydrogenation over the 1.0% Ru/D catalyst. However, as hydrogen uptake progresses, a decrease in the reaction rate is observed due to coverage of the catalyst surface by products and intermediate species. Table 2 shows the extent of toluene hydrogenation and the distribution of products over the 1.0% Ru/D catalyst at different temperatures.

Table 2. Results of Toluene Hydrogenation over 1.0% Ru/D Catalyst at Different Temperatures.

Temperature, °C	Conversion, %	Product Distribution, %		
		Methylcyclohexane	Dimethylcyclopentane	Toluene
90	50.0	60	0	40
110	55.0	54	1	45
130	60.0	58	2	40

As shown in Table 4, toluene conversion increases with temperature: at 90 °C, the conversion reaches 40%, with methylcyclohexane as the main product (60%) and no detectable dimethylcyclopentane. At 110 °C, the conversion rises to 55%, with methylcyclohexane accounting for 54% and a small amount of isomerization observed (dimethylcyclopentane 1%). At 130 °C, the conversion further increases to 60%, methylcyclohexane yield reaches 58%, and the dimethylcyclopentane content rises to 2%. This indicates that at higher temperatures, alongside the

https://doi.org/10.66973/jees.26.003

main hydrogenation pathway, isomerization reactions become more pronounced, although methylcyclohexane remains the predominant primary product.

3.4 Hydrogenation of o-Xylene

Hydrogenation experiments of o-xylene were carried out over a 1.0% Ru/D catalyst at 90 °C under 1 MPa hydrogen pressure (800 rpm) in an ethanol solvent. The results of the hydrogenation are presented in Figure 9.

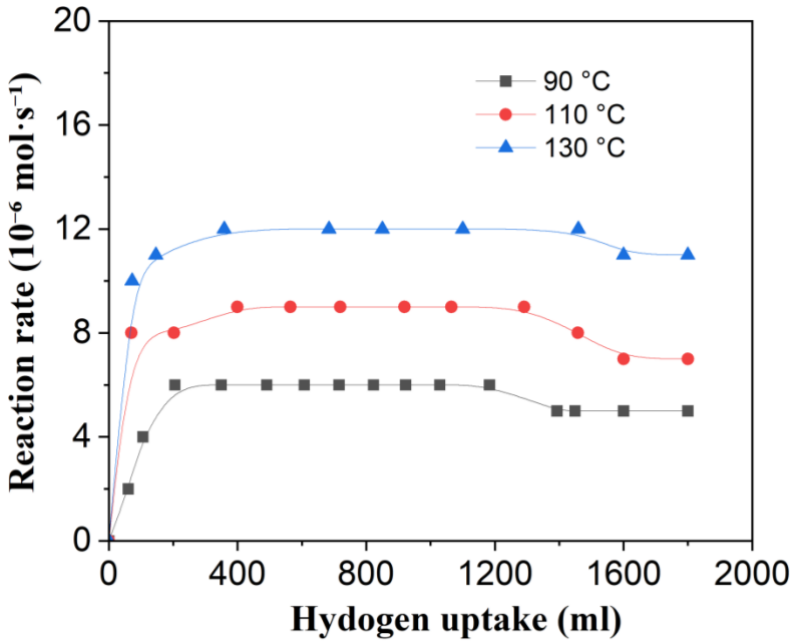

Figure 9. Dependence of the reaction rate on hydrogen uptake during o-xylene hydrogenation over 1.0% Ru/D catalyst at different temperatures.

During o-xylene hydrogenation over the 1.0% Ru/D catalyst, the reaction rate rises sharply with hydrogen uptake, reaching a maximum at approximately 200–300 mL, followed by a gradual decline at very high hydrogen uptake volumes (≈1300–1800 mL). Raising the temperature from 90 °C to 110 and 130 °C markedly increases the reaction rate across the entire hydrogen uptake range, indicating that kinetic limitations are reduced at higher temperatures and that the turnover of hydrogen and o-xylene molecules on the catalyst surface is accelerated.

Although the overall mechanism is analogous to that of benzene and toluene hydrogenation, including dissociative adsorption of H_2, π-complex adsorption of the aromatic ring, stepwise hydrogenation, and subsequent product desorption, the hydrogenation of o-xylene proceeds more slowly and shows a greater dependence on temperature.

As shown in Table 3, at 90 °C the conversion of o-xylene reaches 35%, with the main products being dimethylcyclohexane and trimethylcyclopentane (35%), while no isomers are detected. When the temperature is increased to 110 °C, the conversion rises to 46%, with hydrogenation products accounting for 45% and isomers for 1%. At 130 °C, the conversion further increases to 52%, with hydrogenation products reaching 50% and isomers 2%, while the remaining o-xylene accounts for 48%.

https://doi.org/10.66973/jees.26.003

Table 3. Results of o-xylene hydrogenation over 1.0% Ru/D catalyst at different temperatures.

Temperature, °C	Conversion, %	Product distribution, %		
		Hydrogenation product (dimethylcyclohexane and trimethylcyclopentane)	Isomer (m-xylene and p-xylene)	o-Xylene
90	35.0	35.0	0	65.0
110	46.0	45.0	1.0	54.0
130	52.0	50.0	2.0	48.0

Thus, with increasing temperature, both the overall conversion and the yield of hydrogenation products increase, whereas the isomerization pathway remains very limited (0 to 2%). This indicates that the Ru/D catalyst predominantly promotes hydrogenation of the aromatic ring, while the isomerization of o-xylene to m- and p-xylene represents only a minor side reaction.

From a mechanistic point of view, the hydrogenation of o-xylene proceeds via π adsorption of the aromatic ring on the Ru surface followed by stepwise hydrogen addition. The principal products are dimethylcyclohexane, formed through ring hydrogenation, and a small amount of trimethylcyclopentane resulting from ring contraction. With increasing temperature, a small fraction of molecules undergoes isomerization to form m- and p-xylene (0 to 2%). However, because this pathway is energetically less favorable, hydrogenation remains the dominant reaction route.

3.5 Hydrogenation of a benzene, toluene, and o-xylene mixture over a 1.0% Ru/D catalyst.

Hydrogenation reactions of benzene in the presence of aromatic compounds were carried out over the 1.0% Ru/D catalyst at 90 °C under a hydrogen pressure of 1 MPa (800 rpm) using ethanol as a solvent. The results of the hydrogenation are presented in Figure 10.

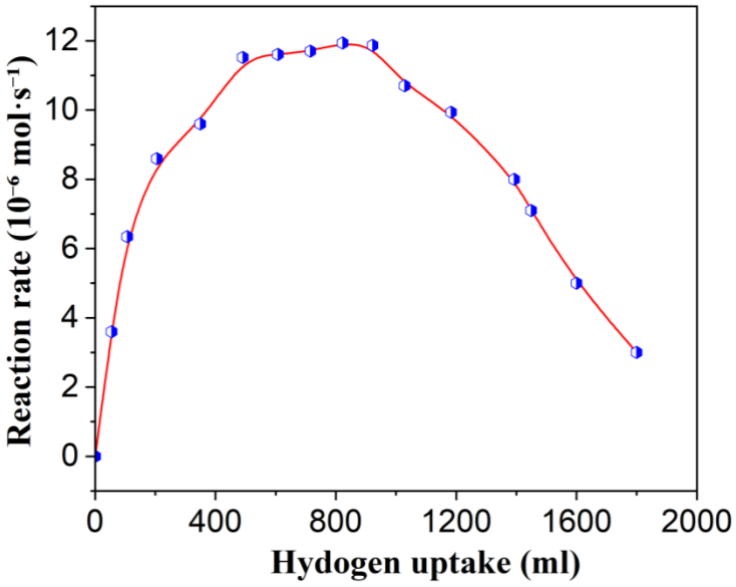

Figure 10. Dependence of the reaction rate on hydrogen uptake during hydrogenation of a benzene, toluene, and xylene mixture over the 1.0% Ru/D catalyst at 90 °C.

https://doi.org/10.66973/jees.26.003

As shown in the figure 10, during hydrogenation of the benzene, toluene, and xylene mixture over the 1.0% Ru/D catalyst at 90 °C, the reaction rate initially increases rapidly with hydrogen uptake. In the range of 0–300 mL, the rate rises from zero to approximately 9×10^{-6} mol s^{-1}. Between 400 and 800 mL of hydrogen uptake, the reaction rate reaches a maximum of about $11.5–12\times10^{-6}$ mol.s^{-1} and forms a plateau, indicating optimal surface coverage of hydrogen for this catalytic system.

As hydrogen uptake further increases from 900 to 1900 mL, the reaction rate gradually decreases to approximately 3×10^{-6} mol·s^{-1}. This decline can be attributed to the decreasing concentration of aromatic substrates, as well as partial coverage of the catalyst surface by reaction products such as cyclohexane and alkylcyclohexanes, and by excess hydrogen, which reduces the availability and effectiveness of active sites. Thus, in this system, the reaction rate reaches its maximum at an intermediate level of hydrogen uptake, whereas further hydrogen absorption does not accelerate the process and instead leads to a gradual decrease in the reaction rate.

Table 4 presents the results of hydrogenation of a benzene, toluene, and o-xylene mixture over the 1.0% Ru/D catalyst: the conversion of benzene reaches 94%, while the conversions of toluene and o-xylene are 14% and 2%, respectively.

Table 4. Results of benzene hydrogenation in the presence of aromatic compounds over the 1.0% Ru/D catalyst at 90 °C.

Conversion, %		
benzene	toluene	o-xylene
94.0	14.0	2.0

These results confirm the high selectivity of the catalyst toward benzene. Benzene is almost completely converted to cyclohexane (94%), whereas toluene and o-xylene largely remain unreacted. This behavior can be attributed to differences in adsorption strength on the Ru surface: as a symmetrical molecule, benzene forms a stable π-complex with the Ru sites, allowing it to adsorb more strongly and effectively displace methyl-substituted aromatics under competitive adsorption conditions.

The steric hindrance and electron-donating effect of the methyl groups weaken the adsorption of toluene and o-xylene. Consequently, the reactivity decreases in the order benzene > toluene > o-xylene. After hydrogenation, the products desorb into the solution, leaving free active sites on the catalyst surface, which are subsequently occupied again by benzene molecules, allowing the catalytic cycle to continue.

Thus, when a mixture of aromatics is hydrogenated over the Ru/D catalyst, the combined effects of adsorption strength, steric hindrance, and electronic factors result in preferential and nearly complete hydrogenation of benzene, whereas toluene and o-xylene are hydrogenated only to a minor extent. This leads to an overall shift in the system's selectivity toward benzene hydrogenation.

4 Conclusion

Ruthenium nanoparticles supported on diatomite (Ru/D) were successfully prepared with high dispersion while preserving the support morphology. Characterization confirmed uniform Ru distribution, minimal structural changes, and only slight decreases in surface area and pore volume with increasing metal loading. Catalytic tests showed that benzene hydrogenation proceeded efficiently, whereas hydrogenation of toluene and o-xylene was slower due to steric and electronic effects. In mixed-aromatic systems, the catalyst exhibited pronounced selectivity toward benzene, highlighting the influence of adsorption strength and molecular structure on competitive reactions. Increasing Ru loading enhanced the number of active sites and overall reaction rates without compromising the integrity of the diatomite framework. These results demonstrate that Ru/D catalysts provide a favorable

combination of high activity, selectivity, and structural stability.

Funding
This research received no external funding.

Author Contributions
A.M.: Methodology, Software, Writing – Original Draft.
R.A. and K.T.: Supervision, Conceptualization, Writing – Review & Editing.

Ethics Approval and Consent to Participate
This study did not involve human participants or animals. Therefore, ethical approval and informed consent were not required.

Data Availability Statement
The data supporting the findings of this study are available from the corresponding author upon reasonable request.

Supporting Information
Not applicable.

Conflict of Interest
The authors declare no conflict of interest.

AI Use Disclosure
The authors confirm that No AI tools were used to generate scientific results, data, figures, or interpretations. All analyses, conclusions, and scientific content were developed by the authors.

REFERENCES:

[1] E. N. Al-Shafei, M. Z. Albahar, M. F. Aljishi, A. Akah, A. N. Aljishi, and A. Alasseel, "Catalytic conversion of heavy naphtha to reformate over the phosphorus-ZSM-5 catalyst at a lower reforming temperature," *RSC Advances*, vol. 12, no. 39, pp. 25465–25477, 2022, doi: https://doi.org/10.1039/d2ra04092a.

[2] Z. Wang, M. Ke, Z. Song, J. Li, and J. Sun, "Benzene Reduction Process Simulation and Optimization in Catalytic Cracking Gasoline Distillation," *Processes*, vol. 11, no. 1, p. 151, Jan. 2023, doi: https://doi.org/10.3390/pr11010151.

[3] F. Velázquez-Alonso *et al.*, "Operative Improvement in the Naphtha Catalytic Reforming Process to Reduce the Environmental Impact of Benzene Fugitive Emissions from Gasoline," *ChemEngineering*, vol. 9, no. 2, pp. 21–21, Feb. 2025, doi: https://doi.org/10.3390/chemengineering9020021.

[4] IARC Working Group on the Evaluation of Carcinogenic Risks to Humans, "Some non-heterocyclic polycyclic aromatic hydrocarbons and some related exposures," *IARC monographs on the evaluation of carcinogenic risks to humans*, vol. 92, pp. 1–853, 2010, Accessed: Jul. 23, 2024. [Online]. Available: https://pubmed.ncbi.nlm.nih.gov/21141735/

[5] A. B. Patel, S. Shaikh, K. R. Jain, C. Desai, and D. Madamwar, "Polycyclic Aromatic Hydrocarbons: Sources, Toxicity, and Remediation Approaches," *Frontiers in Microbiology*, vol. 11, no. 11, Nov. 2020, doi: https://doi.org/10.3389/fmicb.2020.562813.

[6] C. Fan, Y.-A. Zhu, X.-G. Zhou, and Z.-P. Liu, "Catalytic hydrogenation of benzene to cyclohexene on Ru(0001) from density functional theory investigations☆," *Catalysis Today*, vol. 160, no. 1, pp. 234–241, Feb. 2011, doi: https://doi.org/10.1016/j.cattod.2010.03.075.

[7] D. Zhao, J. Meng, and X. Lin, "Mathematical modelling of simultaneous hydrogenation of benzene and ethane dehydrogenation in a membrane reactor," *Case Studies in Thermal Engineering*, vol. 71, p. 106133, Jul. 2025, doi: https://doi.org/10.1016/j.csite.2025.106133.

[8] E. A. Dada and Luke E.K. Achenie, "Production of Cylohexane from Hydrogenation of Benzene using Microreactor Technology," *Computer-aided chemical engineering*, vol. 31, pp. 240–244, Jan. 2012, doi: https://doi.org/10.1016/b978-0-444-59507-2.50040-8.

[9] F. Hao *et al.*, "Preparation of mesoporous SiO2–Al2O3 supported Co or Mn catalysts and their catalytic properties in cyclohexane nitrosation to ε-caprolactam," *Journal of Molecular Catalysis A: Chemical*, vol. 351, pp. 210–216, Dec. 2011, doi: https://doi.org/10.1016/j.molcata.2011.10.010.

[10] P. Modisha and D. Bessarabov, "Aromatic liquid organic hydrogen carriers for hydrogen storage and release," *Current Opinion in Green and Sustainable Chemistry*, vol. 42, p. 100820, Apr. 2023, doi: https://doi.org/10.1016/j.cogsc.2023.100820.

[11] C. Chu, K. Wu, B. Luo, Q. Cao, and H. Zhang, "Hydrogen storage by liquid organic hydrogen carriers: Catalyst, renewable carrier, and technology - A review," *Carbon Resources Conversion*, vol. 6, no. 4, pp. 334–351, Mar. 2023, doi: https://doi.org/10.1016/j.crcon.2023.03.007.

[12] W. Gu *et al.*, "Benzene Selectivity in Competitive Arene Hydrogenation: Effects of Single-Site Catalyst···Acidic Oxide Surface Binding Geometry," *Journal of the American Chemical Society*, vol. 137, no. 21, pp. 6770–6780, Apr. 2015, doi: https://doi.org/10.1021/jacs.5b03254.

[13] L. M. Kustov, A. L. Tarasov, A. L. Kustov, and O. P. Tkachenko, "Enhancement of Efficiency of Pd/Al2O3Catalysts in Selective Hydrogenation of Sec-Butylbenzene by Modification with H_2SO_4 or H_2WO_4," *Metals*, vol. 11, no. 2, p. 281, Feb. 2021, doi: https://doi.org/10.3390/met11020281.

[14] L. Foppa and J. Dupont, "Benzene partial hydrogenation: advances and perspectives," *Chemical Society Reviews*, vol. 44, no. 7, pp. 1886–1897, Jan. 2015, doi: https://doi.org/10.1039/C4CS00324A.

[15] B. Taleb *et al.*, "Exploring Hydrogen Sources in Catalytic Transfer Hydrogenation: A Review of Unsaturated Compound Reduction," *Molecules*, vol. 28, no. 22, p. 7541, Nov. 2023, doi: https://doi.org/10.3390/molecules28227541.

[16] M. Johansson, O. Lytken, and I. Chorkendorff, "The sticking probability for H2 on some transition metals at a hydrogen pressure of 1bar," *The Journal of Chemical Physics*, vol. 128, no. 3, p. 034706, Jan. 2008, doi: https://doi.org/10.1063/1.2825296.

[17] Z. Mohammadian and N. Parsafard, "Optimization of Kinetic Study by Response Surface Methodology on the Various Types Ni Supported Catalysts in Competitive Benzene Hydrogenation," *Theoretical Foundations of Chemical Engineering*, vol. 56, no. 6, pp. 1179–1188, Dec. 2022, doi: https://doi.org/10.1134/s0040579522330053.

[18] R. Molina and G. Poncelet, "Hydrogenation of Benzene over Alumina-Supported Nickel Catalysts Prepared from Ni(II) Acetylacetonate," *Journal of Catalysis*, vol. 199, no. 2, pp. 162–170, Apr. 2001, doi: https://doi.org/10.1006/jcat.2001.3169.

[19] I. S. Mashkovsky, G. N. Baeva, A. Yu. Stakheev, T. V. Voskoboynikov, and P. T. Barger, "Pd/Al2O3 catalyst for selective hydrogenation of benzene in benzene–toluene mixture," *Mendeleev Communications*, vol. 19, no. 2, pp. 108–109, Mar. 2009, doi: https://doi.org/10.1016/j.mencom.2009.03.020.

[20] Aleksandr Glotov *et al.*, "Ruthenium Catalysts Templated on Mesoporous MCM-41 Type Silica and Natural Clay Nanotubes for Hydrogenation of Benzene to Cyclohexane," *Catalysts*, vol. 10, no. 5, p. 537, May 2020, doi: https://doi.org/10.3390/catal10050537.

[21] H. Sun *et al.*, "Selective Hydrogenation of Benzene to Cyclohexene over Ru-Zn Catalysts: Investigations on the Effect of Zn Content and ZrO2 as the Support and Dispersant," *Catalysts*, vol. 8, no. 11, p. 513, Nov. 2018, doi: https://doi.org/10.3390/catal8110513.

[22] K. Toshtay *et al.*, "Effect of Catalyst Preparation on the Selective Hydrogenation of Vegetable Oil Over Low Percentage Pd/Diatomite Catalysts," *Eurasian Chemico-Technological Journal*, vol. 17, no. 1, pp. 33–39, 2015, doi: https://doi.org/10.18321/ectj192.

[23] K. Toshtay, "Liquid-phase hydrogenation of sunflower oil over platinum and nickel catalysts: Effects on activity and stereoselectivity," *Results in Engineering*, vol. 21, p. 101970, Mar. 2024, doi: https://doi.org/10.1016/j.rineng.2024.101970.

[24] S. J. Gregg and W. Sing, *Adsorption, Surface Area, and Porosity*, 2nd ed. London: Academic Press, 1982.

[25] K. Toshtay and A. B. Auezov, "Hydrogenation of Vegetable Oils over a Palladium Catalyst Supported on Activated Diatomite," *Catalysis in Industry*, vol. 12, no. 1, pp. 7–15, Jan. 2020, doi: https://doi.org/10.1134/s2070050420010109.

[26] R. Zheng, Z. Ren, H. Gao, A. Zhang, and Z. Bian, "Effects of calcination on silica phase transition in diatomite," *Journal of Alloys and Compounds*, vol. 757, pp. 364–371, Aug. 2018, doi: https://doi.org/10.1016/j.jallcom.2018.05.010.

[27] D. Li *et al.*, "Characterizations and performances of Ni/diatomite catalysts for methane decomposition to obtain carbon nanotubes and high-purity H2," *International Journal of Hydrogen Energy*, vol. 109, pp. 732–741, Mar. 2025, doi: https://doi.org/10.1016/j.ijhydene.2024.12.386.

[28] N.-S. Mussa, Kanat Amantaiuly, Seitkhan Azat, Rachid Amrousse, and Kainaubek Toshtay, "Modification of Diatomite Mineral Sorbent for the Cleanup of Petroleum Spills on Water Surfaces," *Eurasian Chemico-Technological Journal*, vol. 27, no. 2, pp. 101–110, Jul. 2025, doi: https://doi.org/10.18321/ectj1658.

[29] M. A. Keane and P. M. Patterson, "Compensation behaviour in the hydrogenation of benzene, toluene and o-xylene over Ni/SiO2. Determination of true activation energies," *Journal of the Chemical Society, Faraday Transactions*, vol. 92, no. 8, pp. 1413 – 1421, 1996, doi: https://doi.org/10.1039/ft9969201413.

[30] S. LU *et al.*, "Low temperature hydrogenation of benzene and cyclohexene: A comparative study between γ-Al2O3 supported PtCo and PtNi bimetallic catalysts," *Journal of Catalysis*, vol. 259, no. 2, pp. 260–268, Oct. 2008, doi: https://doi.org/10.1016/j.jcat.2008.08.016.

[31] H. Nagahara, M. Ono, M. Konishi, and Y. Fukuoka, "Partial hydrogenation of benzene to cyclohexene," *Applied Surface Science*, vol. 121–122, pp. 448 – 451, Nov. 1997, doi: https://doi.org/10.1016/S0169-4332(97)00325-5.

[32] G. Zhong, B. Chan, and L. Radom, "Hydrogenation of Simple Aromatic Molecules: A Computational Study of the Mechanism," *Journal of the American Chemical Society*, vol. 129, no. 4, pp. 924–933, Jan. 2007, doi: https://doi.org/10.1021/ja066251a.